Elementary Relativistic Atoms

Leonid Nemenov

[1] Joint Institute for Nuclear Research, 141980 Dubna, Moscow Region, Russia
[2] CERN, CH-1211 Geneva 23, Switzerland

Abstract. The Coulomb interaction which occurs in the final state between two particles with opposite charges allows for creation of the bound state of these particles. In the case when particles are generated with large momentum in lab frame, the Lorentz factors of the bound state will also be much larger than one. The relativistic velocity of the atoms provides the oppotrunity to observe bound states of $(\pi^+\mu^-)$, $(\pi^+\pi^-)$ and (π^+K^-) with a lifetime as short as 10^{-16} s, and to measure their parameters. The ultrarelativistic positronium atoms (A_{2e}) allow us to observe the effect of superpenetration in matter, to study the effects caused by the formation time of A_{2e} from virtual e^+e^- pairs and to investigate the process of transformation of two virtual particles into the bound state.

1 Introduction

In all processes, when there are two free particles a^+ and b^- in the final state, there is also some probability that the bound state of these particle, A_{ab}, will also be present.

The mechanism of A_{ab} creation is the Coulomb interaction in the final state (between a^+ and b^-), formatting from two virtual particles a^+ and b^-, the bound state A_{ab} (Fig. 1). This mechanism, in principle, allows for creation of all types of bound states and if a^+ and b^- are relativistic particles, then A_{ab} will also be relativistic. For ultra-relativistic atoms, there are effects caused by final time of atom formation and new phenomena during atom interaction with matter. High value of the Lorentz factors of atoms also allows for the detection new short lived bound states $A_{\pi\mu}$, $A_{2\pi}$ and $A_{\pi K}$, consisting accordingly from $(\pi^+\mu^-)$, $(\pi^+\pi^-)$ and (π^+K^-) mesons and to measure their parameters.

Presented in this review are those processes which are connected with observed relativistic atoms. The decay

$$K_L^0 \to A_{\pi\mu} + \nu \,, \tag{1}$$

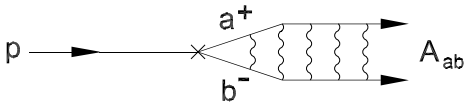

Fig. 1. Formation of the A_{ab} bound state of two charged particles a^+ and b^- due to the Coulomb interaction in the final state

which is a source of the relativistic $A_{\pi\mu}$ [1] is described in section 2. This decay and the relativistic $A_{\pi\mu}$ were observed in 1976 by M.Schwartz and collaborators [2] and the probability (1) was measured [3]. The measurement of the energy difference between $2P_{1/2}$ and $2S_{1/2}$ $A_{\pi\mu}$ levels gives the value of the pion charge radius.

In section 3 the decay

$$\pi^0 \to \gamma + \text{positronium} , \tag{2}$$

which is a source of the ultra-relativistic positronia [4] is described. Decay (2) and ultra-relativistic positronium (A_{2e}) with Lorentz factors $800 \leq \gamma \leq 2000$ were observed in 1984 [5]. The measurement of the probability (2) and the cross section for interaction of ultra-relativistic A_{2e} with carbon were made accordingly in [6] and [7].

At high values of Lorentz factors the probability of passage of an atom through a layer of matter becomes greater than the one that follows from the usual exponential dependence. This phenomenon was predicted in [8] and was given the name "superpenetration". The quantitative theory of superpenetration was developed in [9,10,11]. For ultrarelativistic A_{2e}, the time of formation from the virtual electron-positron pair is strongly dependent on the thickness of the target [12].

Taking into account the time of formation A_{2e} from the virtual electron-positron pair for ultrarelativistic A_{2e} changes very strongly the effective value of the thickness of target for A_{2e} production [12].

This effect allows for production relatively intense beams of ultrarelativistic positronium by photons with energy within 10–100 GeV.

Section 4 describes the atoms consisting of π^+ and π^- mesons ($A_{2\pi}$) and experiments involving their detection and lifetime measurement. The lifetime of $A_{2\pi}$ is determined by the charge-exchange process

$$\pi^+\pi^- \to \pi^0\pi^0 \tag{3}$$

at the threshold and connects with a precise relationship [13,14,15,16,17] to pion-pion scattering lengths in S-state with isotope spin 0 and 2 (a_0, a_2). The measurement of the lifetime of $A_{2\pi}$ allows one to determine the difference $|a_0 - a_2|$ in a model independent way.

These parameters can be evaluated using effective Lagrangian and Chiral Perturbation Theory [18,19,20,21,22] which is mathematically equivalent to QCD [19,21]. At present time, the value $a_0 - a_2$ has been determined within 2% [23]. The QCD Lagrangian and effective Lagrangians are determined by Lorentz invariance, P and C-invariance and by the chiral symmetry. For this reason, the measurement of $|a_0 - a_2|$ provides an opportunity to check our understanding of the chiral symmetry breaking of QCD.

Many years ago it was assumed [24,25] that the spontaneous breaking of chiral symmetry is due to a strong condensation of quark-antiquark pairs in vacuum. A scenario alternative to the standard case – with a weak quark condensation – was also considered [26,27,28,29] and the values of a_0, a_2 were obtained. The

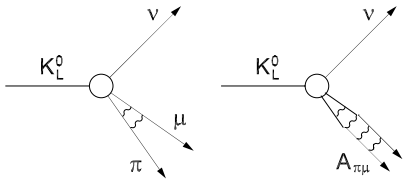

Fig. 2. K_L^0 decay with production of three free particles (left) and the same decay with formation of the $A_{\pi\mu}$ bound state due to the Coulomb interaction (right)

measurement of $a_0 - a_2$ provides the possibility for one to make some conclusions about the value of the quark condensate.

The method for $A_{2\pi}$ observation and the lifetime measurement were proposed in [30]. In 1994 $A_{2\pi}$ were observed and a lower limit estimation of their lifetime was given [31,32]. In 1999 the detection of $A_{2\pi}$ was performed in the DIRAC experiment at CERN and the measurement of $a_0 - a_2$ with 5% precision is planned for 2002–2003. Also present in section 4 is brief information about atoms, consisting of π^+ and K^- $(A_{\pi K})$ [30,33] and $A_{2\pi}$ production in the decays [34].

2 Atoms consisting of π and μ mesons

Investigation of atoms consisting of π and μ mesons $(A_{\pi\mu})$, in principle, allows one to obtain the pion charge radius in a model independent way.

2.1 $A_{\pi\mu}$ properties

The basic properties of $A_{\pi\mu}$ are calculable with the formalism used to describe the hydrogen atom. The reduced mass of the system is $60.2\,\mathrm{MeV}/c$, its Bohr radius is $4.5 \cdot 10^{-11}\,\mathrm{cm}$, and the binding energy of the $1S_{1/2}$ state is $1.6\,\mathrm{keV}$. These atoms are produced in the decay (1) of K_L^0 mesons (Fig. 2).

The branching ratio

$$R = \frac{K_L^0 \to A_{\pi\mu} + \nu}{K_L^0 \to \pi + \mu + \nu} \tag{4}$$

was calculated in [1,35]. Corrections to (4) taking into account the effects of the finite size of the pion (0.4%), vacuum polarization (0.2%) and the first order relativistic correction to the atomic wave function were obtained in [36]. The final value of R [3] is

$$R = (4.31 \pm 0.08) \cdot 10^{-7}\,. \tag{5}$$

The value R is proportional to the square of the $A_{\pi\mu}$ wave function at small distances and so an anomaly in its value may be indicative of an anomaly in the $\pi\mu$-interaction [2,35]. The difference between the energy of the $2P_{1/2}$ and $2S_{1/2}$ states (Lamb shift) neglecting pion size corrections is $\Delta E = 79.45 \cdot 10^{-3}\,\mathrm{eV}$.

The finite size of the pion gives an additional 0.5 to $1.0 \cdot 10^{-3}\,\mathrm{eV}$, [37,38,39,40] which means that a measurement of the $2P_{1/2} - 2S_{1/2}$ splitting could provide

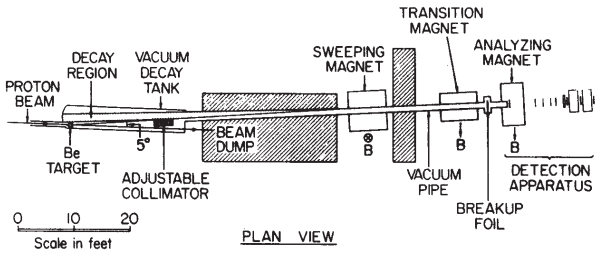

Fig. 3. Experimental arrangement for observation of the decay $K_L^0 \to A_{\pi\mu} + \nu$

an independent measurement of the pion charge radius [2,3]. By passage of the $A_{\pi\mu}$ through a magnetic field with Lorentz factor $\gamma > 10$ the $2S$ state should be depopulated through electric field mixing with $2P$ states and consequent decay to the $1S$ state. The extent of this depopulation will be highly dependent upon the vacuum polarization shift of $2S$ states relative to the $2P$ states and may if measured with some accuracy, lead to a determination of the pion charge radius.

2.2 Observation of $A_{\pi\mu}$

Atoms consisting of a negative (or positive) pion and a positive (or negative) muon were observed in [2]. In this experiment the 30 GeV proton beam strikes a 10 cm beryllium target (Fig. 3). A 4 ft steel collimator prevents any direct line of sight from the detector system to the target. This is to prevent background particles, in particular K_L^0's, from approaching the neighbourhood of detectors. Those K_L^0's which decay within the "decay region" give rise to decay products which travel down the channel. In order to remove charged particles there were two magnets along this channel. After these magnets, the beam consists of γ rays, highly energetic pions and muons and occasional atoms. The momentum spectrum of the atoms coming down the channel has no appreciable contribution above 5 GeV/c. To make the atoms detection possible thin aluminium foils (l = 0.030 in. and 0.250 in) were interposed just before the end of the vacuum channel. After atom ionization, the uncoupled pion and muon exit from the foil at the same velocity with small opening angle. The analyzing magnet separated the pion and muon in the vertical plane, and the set of detectors measured the momentum of the particles and identified their type.

After the introduction of a set of criteria, 33 events were found. For each of these events the parameter

$$\alpha = \frac{P_\pi - P_\mu}{P_\pi + P_\mu} \tag{6}$$

was plotted, where P_π, P_μ are the pion and muon momentum. The apparatus acceptance was flat in the region $0.4 \leq \alpha \leq -0.4$. Hence, any bump in this plot would indicate a strong correlation between pion and muon momenta.

For the particles from $A_{\pi\mu}$ breaking $\alpha = 0.14$. The data shows a clear peak at the predicted point (Fig. 4(a)) containing a total of 21 events with an estimated

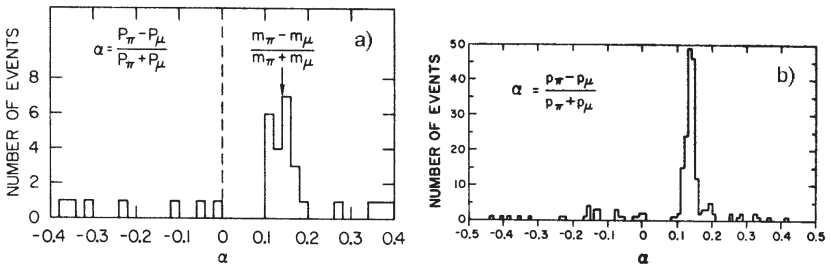

Fig. 4. (a) Plot of parameter α, indicating the first detection of $\pi\mu$-atoms; (b) the same plot obtained in the experiment on measurement of the $A_{\pi\mu}$ formation rate in K_L^0 decay

background of three events. It was the first observation of atoms, created by Coulomb interaction in the final state, and consisting of two unstable particles.

2.3 Measurement of the $A_{\pi\mu}$ formation rate in K_L^0 decay

To perform the experiment [41] an intense beam of high-energy K_L^0 was constructed at Fermilab. After the 400 GeV/c proton beam struck a beryllium target, a series of collimators and magnets defined the beam and swept charged particles from the flux of secondaries emerging in the forward direction (Fig. 5). The average K_L^0 momentum was about 75 GeV/c, and typical intensities were about 10^7 K_L^0's and 10^9 neutrons per accelerator pulse. The setup detected the pions and muons from the decay

$$K_L^0 \to \pi + \mu + \nu \tag{7}$$

and pions and muons from the $A_{\pi\mu}$ breaking through the aluminium foils that had a thickness of $l = 0.020$ in and $l = 0.035$ in. In order to distinguish pions and muons from decay (7) and from the $A_{\pi\mu}$ dissociation (atomic pairs) a horizontal magnetic field prior to the foil was introduced. This magnet caused the charged particles from (7) to have vertically separated trajectories but neutral objects, such as $A_{\pi\mu}$ and photons passed through this magnet unperturbed. The first magnet installed after the aluminium foil separated the particles horizontally, and the second magnet (analyzing magnet) restored the parallelism of the particles trajectories, simplifying the trigger organization.

The analyzing magnet in conjunction with the multi-wire proportional chamber planes, was used to measure the momenta of charged particles. The shower counters and scintillation counters, installed after the iron absorbers, identified electrons and muons accordingly. After the introduction of a set of criteria, 320 examples of the decay (1) were observed. By imposing more strict criteria, from this number, 163 events were selected [3].

The distribution of these events on the parameter L is presented on Fig. 4(b). Using these events the R value was measured

$$R = (3.90 \pm 0.39) \cdot 10^{-7} \,. \tag{8}$$

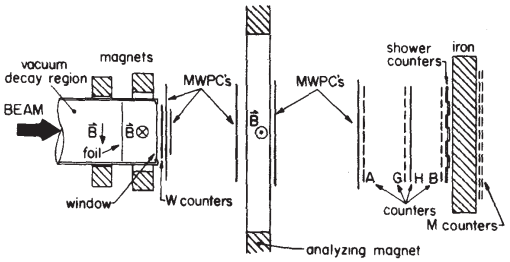

Fig. 5. Plan of the detection apparatus for measurement of the $A_{\pi\mu}$ formation rate in K_L^0 decay

For obtaining (8) it was assumed that the $A_{\pi\mu}$ lifetime is determined by the pion and muon lifetimes.

This number is in agreement with the theoretical prediction calculated on the assumption that the interaction between the muon and the pion is the Coulomb interaction: $R_{\rm exp}/R_{\rm th} = 0.905 \pm 0.091$

3 Ultrarelativistic positronium atoms (A_{2e})

The ultrarelativistic A_{2e} allows one to observe the new effects concerning the positronium interactions with matter and the final value of the formation time of an atom from an e^+e^--pair.

3.1 Source of the ultrarelativistic A_{2e} and their quantum numbers

At present, the ultrarelativistic A_{2e} have been only observed in the process in which a time-like photon γ is converted into a bound state of the electron and positron (Fig. 6(c)). If in the radiative process (Fig. 6(a)) where a, b are the particles and γ is the photon

$$\mathrm{a} \to \mathrm{b} + \gamma\ . \tag{9}$$

The γ energy is much greater than the positronium mass, and the branching ratio for the atomic decay

$$\mathrm{a} \to \mathrm{b} + A_{2e} \tag{10}$$

is almost independent of the masses and kinds of particles a, b and is equal to [4]:

$$\rho_A = \frac{W(\mathrm{a} \to \mathrm{b} + A_{2e})}{W(\mathrm{a} \to \mathrm{b} + \gamma)} = 0.30\ \alpha^4 = 0.84 \cdot 10^{-9} \tag{11}$$

The radiative correction for the value of ρ_A has been calculated [42].

The main source of ultrarelativistic A_{2e} from proton accelerators is the π^0 decay :

$$\pi^0 \to \gamma + A_{2e} \tag{12}$$

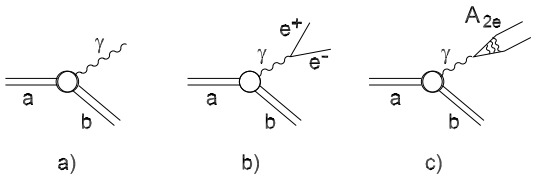

Fig. 6. Diagrams describing the radiative decay (a), the decay with a free e^+e^--pair in the final state (b) and conversion of a time-like photon to the positronium

with probability $\rho_\pi = 2\rho_A = 1.69 \cdot 10^{-9}$. The intensity of relativistic positronium beams for high energy proton accelerators with internal beam energies of $13 \div 5000$ GeV, and emission angles in the lab frame in the range from $0°$ to $15°$, was calculated in [43].

The probability of (12) is proportional to the square of the atom wave function at small separations $|\Psi(0)|^2$ and the charged parity of A_{2e} must coincide with the charged parity of the virtual photon. Thus the A_{2e} quantum numbers from (12) are [4]

$$l = 0\,, \qquad s = 1\,, \qquad \text{and} \qquad W_n \sim 1/n^3\,, \tag{13}$$

where l, and s are the atom orbital angular momentum and spin and W_n the probability of A_{2e} production with principal quantum number n. In the transverse magnetic field moving A_{2e} disintegrate if the electric field strength in the A_{2e} rest system is more than a threshold value. [44].

Positronium in the ground state and first exited state ($n = 2$) can exist if his Lorentz factor γ, velocity v ($\beta = v/c$) and the strength H of the magnetic field in the lab frame satisfy the inequality

$$\beta\gamma H < 1.4 \cdot 10^5 \text{ Oe} \;\; (\text{for } n = 1)\,, \quad \beta\gamma H < 1.13 \cdot 10^4 \text{ Oe (for } n = 2)\,. \tag{14}$$

If a positronium beam with $s = 1$ passes through a magnetic field with a strength satisfying condition (14) the probability of A_{2e} dissociation is very small. The atom wave function in the magnetic field will be a superposition of the A_{2e} wave functions in the singlet (short-lived) and triplet (long-lived) state. If beyond the magnet there is a decay gap, then the positronium beam intensity will oscillate as a function of the values of H, γ and the magnet length l because the probability of observing an atom beyond the magnet in the short-lived or long-lived state depends on H, γ and l [45].

3.2 Superpenetration of ultrarelativistic atoms

On moving into the field of an atom, relativistic positronium can break up or be excited. The probabilities of these processes were calculated in [46]. The total cross section for the interaction of relativistic A_{2e} with an atom, σ_{tot}, was also

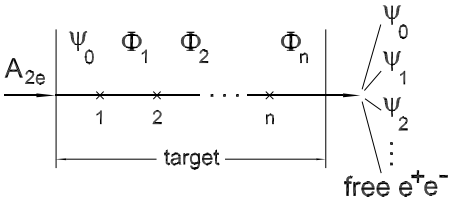

Fig. 7. Positronium in the ground state with the wave function Ψ enters a target and interacts at point 1 with an atom of the target. After the interaction, a non-stationary (e^+e^-) state with the wave function Φ_1 moves in the target and interacts at point 2 with another atom creating a new non-stationary state Φ_2. After the last interaction, a non-stationary (e^+e^-)-system moves to the vacuum and transforms into a set of stationary states: ground and exited states of A_{2e} and free (e^+e^-)-pairs

calculated in [47]. It is practically independent of A_{2e} energy for $\gamma > 10$ and is satisfactorily described by the formula

$$\sigma_{\rm tot} = 0.94\, Z^{1.24} \cdot 10^{-19}\,{\rm cm}^2/{\rm atom}\,, \tag{15}$$

where Z is the atom charge.

For the exponential absorption law the characteristic thickness λ within which the positronium beam intensity is reduced by a factor e has the following values for carbon, molybdenum and platinum

$$\lambda_{\rm C} = 0.14\,\mu{\rm m}\,, \quad \lambda_{\rm Mo} = 1.9 \cdot 10^{-2}\,\mu{\rm m}\,, \quad \text{and} \quad \lambda_{\rm Pt} = 7 \cdot 10^{-3}\,\mu{\rm m}\,. \tag{16}$$

But at high γ factors there is a qualitative change in the nature of the atom interaction with condensed matter. In [8] attention was given to the fact that at sufficiently high values of γ the time t of passage of A_{2e} across the target can become smaller than the characteristic atomic time in the lab frame:

$$t \ll \gamma\,\tau_0\,, \tag{17}$$

where τ_0 is atomic unity of time and for A_{2e} equals $\tau_0 = 4.8 \cdot 10^{-17}$ s. Let the thickness of the carbon film be $L = 10\lambda_{\rm C} = 1.4\,\mu$m and hence $t = 5{\cdot}10^{-15}$ s. Then (17) will be satisfied at $\gamma \geq 10^3$. For these conditions, the wave function which describes e^+e^- in matter will change only under the influence of interactions with the atoms of the absorber. The interaction between the particles of the e^+e^- system leaves the state of the system practically unchanged in a time t (Fig. 7).

In this case the probability of the passage of an atom through a layer of matter becomes greater than the one that follows from the usual exponential dependence. This phenomenon, superpenetration of ultrarelativistic A_{2e}, allows for measurement of the time of conversion of a non-stationary state of e^+e^-, formed in the target, to stationary states and to verify the form of the Lorentz transformations for the time [8]. The theory of superpenetration has been formulated in [9,10,11]. A quantitative calculation shows that even for a film thickness $L = 2.5\lambda$ the deviation from an exponential absorption law reaches 100%.

3.3 Time-of-formation effects in production of ultrarelativistic A_{2e}

In addition to the process (2), positronium can also be generated by photons interacting with matter [14,44,48,49].

$$\gamma + A_Z \to A_{2e} + A_Z \; . \tag{18}$$

The cross section for photo-production of positronium on an atom can be satisfactorily approximated by

$$\sigma = 0.57 Z^{1.86} \cdot 10^{-32} \, \mathrm{cm}^2/\mathrm{atom} \; . \tag{19}$$

It follows from (15), (19) and the exponential absorption of A_{2e} in the medium that the total probability of the atom formation and of the atom escape from a target of thickness $l = \lambda$ per one photon is

$$W_C = 1.1 \cdot 10^{-13} \, , \quad W_{Mo} = 4.1 \cdot 10^{-13} \, , \quad \text{and} \quad W_{Pt} = 5.5 \cdot 10^{-13} \; . \tag{20}$$

The atoms yield is not significantly affected by an increase in the target thickness and takes into account the superpenetration of ultrarelativistic A_{2e}.

In [12] the effect of the A_{2e} formation time on the probability of positronium production and observation was investigated. As they interact with atoms, photons also generate (e^+e^-) pairs of positive energy. To distinguish with $\approx 50\%$ probability between A_{2e} with principal quantum number n and a (e^+e^-) pair of positive energy, we have to measure within the center of mass system (c.m.s.) of the pair, the total energy of the particles with a precision equal to the positronium binding energy E_n. The uncertainty relation of energy and time then shows that the required precision will be achieved only if the measurement is made in a time t_n, which is given by

$$t_n \sim \hbar / E_n \; . \tag{21}$$

The time t (time of A_{2e} formation) is measured in the c.m.s. of the pair from the time of its creation. For $\gamma = 10000$ and $n = 1$, the value of time of A_{2e} formation in the lab frame is $t_1 = 10^{-12}$ s. During this time the (e^+e^-) pair will pass the macro-distance $L_1 = 300\,\mu$m in lab frame. At a distance $l \approx 10\,\mu$m there are no A_{2e} and (e^+e^-) pairs with positive energy. We only have a continuum of (e^+e^-) pairs with an uncertainty in their c.m.s. energy and with a wide distribution on the relative momentum in their c.m.s. By moving through the target matters, this continuum smears in the momentum and coordinate space only by interacting with matter, because the inequality (17) is fulfilled and the interaction between (e^+e^-) does not change the state of the pair. After the target, the electro-magnetic interaction between $e^+$and e^- begins to form A_{2e} primarily from the (e^+e^-) pairs with $k \sim k_B$, and $r \sim r_B$, where k_B, r_B are the A_{2e} Bohr momentum and Bohr radius and r – the distance between e^+, e^- in their c.m.s. The probability to obtain pairs with $k \sim k_B$, and $r \sim r_B$, after the target is relatively high because some of the pairs with $k > k_B$ will come to the region $k \sim k_B$ but the coordinate separation for this pair will be more than r_B and will depend on the photon energy E_γ. The calculation of the target

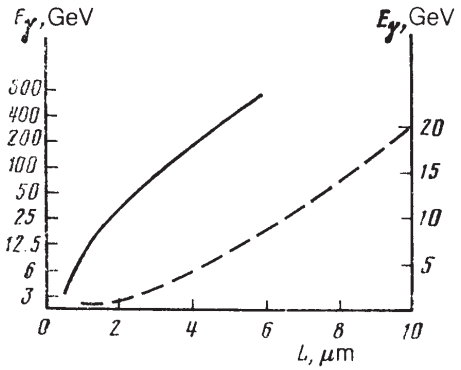

Fig. 8. Photon energy E_γ and platinum thickness that reduce the probability of A_{2e} escape by a factor e (solid curve); the photon energy is shown on the left. The dashed curve shows the corresponding result for carbon; the photon energy is shown on the right

thickness that reduces the probability of A_{2e} escape by a factor e as a function of E_γ is presented in Fig 8. For Pt target and $E_\gamma \sim 10\,\text{GeV}$ this thickness is $\sim$1μm, two orders more than λ_{Pt} from (15) and this value will increase with E_γ [12].

3.4 Observation of ultrarelativistic positronium and measurement of the branching ratio for the π°-mesons decay into a photon and A_{2e}.

The experiments [5,6] were performed on the U-70 accelerator, using the setup, shown in Fig. 9. A target in the form of a carbon film of thickness 0.5 and 0.35 μm was placed in the internal 70 GeV energy proton beam. The main source of ultrarelativistic A_{2e} was the decay (2). The positronium entered a channel located at an angle of 8.4° with respect to the proton beam and connected to the vacuum chamber of the accelerator without diaphragms. The channel length was 40 meters and the solid angle was $2.6 \cdot 10^{-5}$ sr. The channel was terminated by a vacuum chamber placed in the gap of the magnet MP. Along the channel at a distance of $\sim$23 m a horizontal homogeneous magnetic field of 56 Oe strength was applied. This field extracted charged particles with momenta $p < 3\,\text{GeV/c}$ from the beam. The A_{2e} in the ground state with momenta $p < 2.5\,\text{GeV/c}$ passed this weak magnetic field without dissociation and broke into an e^+e^- pair with equal momenta in the strong field of the spectrometer magnet [45]. The e^+ and e^- passed the thin aluminium exit window of the vacuum chamber and were detected by two telescopes consisting of drift chambers (DC), scintillation counters (S) and gas Cherenkov counter (Č) for e^+, e^- identification. The setup detected the A_{2e} with $800 \leq \gamma \leq 2000$.

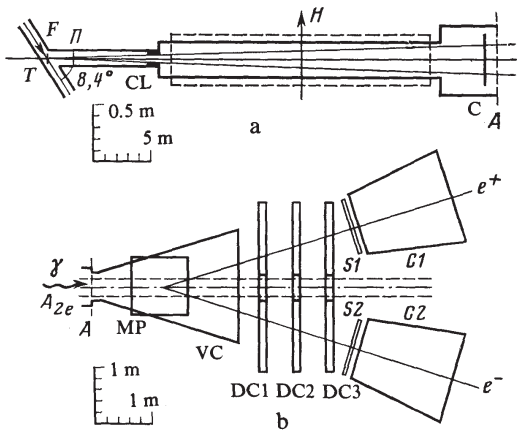

Fig. 9. Experimental setup for observation of ultrarelativistic A_{2e}: a) – channel scheme: p – internal proton beam, T – film target , F – polyester film,CL – collimators, H – horizontal magnetic field, C – plexiglas converter; b) – magnet and detectors: MP – poles of spectrometer magnet, VC – vacuum chamber, DC1, DC2 and DC3 – drift chambers, S1 and S2 – scintillation counters, Č – gas Cherenkov counters

Since there were no coordinate detectors in front of the spectrometer magnet, for determination of the momenta it was assumed that the particles were produced in the carbon target. In this case, using the magnetic field map and coordinate information from DC it is possible to obtain the momenta of e^+ and e^- and their coordinates before the magnet. After tracks construction and introduction of the requirement on the small distance between e^+ and e^- before magnet ($\Delta x < 9\,\text{mm}$, $\Delta y < 3.4\,\text{mm}$) and the condition that the y projection for each track has to point at the target, ∼3800 events were obtained. The distribution of these events on the parameter $\varepsilon = \ln P_{e^+}/P_{e^-}$ is given in Fig. 10. In this distribution there is a narrow peak in the $\epsilon = 0$ region with a total width $\Delta_{\text{exp}} = 2.4\%$ in agreement with the instrumentation resolution $\Delta_{\text{calc}} = 2.3\%$. The number of A_{2e} obtained from the analysis of this distribution and the value of ρ_π are [5]

$$N_{A_{2e}} = 185 \pm 30\,, \qquad \text{and} \qquad \rho_\pi = (1 \div 2) \cdot 10^{-9}\,. \tag{22}$$

The photon and positronium energy spectra are practically the same in any processes with $E\gamma \gg m_e$. Therefore the measurement the A_{2e} to photons ratio at the same momentum and for the same angles range allows one to determine the ρ_A value and hence the branching ratio for decay (12). The measurement was performed on the same setup measuring the number of A_{2e} and the number of photons with the same momenta.

During the run, the ≈0.6 mm ($1.8 \cdot 10^{-3}$ radiation length) plexiglass converter (C) was periodically inserted in the channel before the spectrometric magnet.

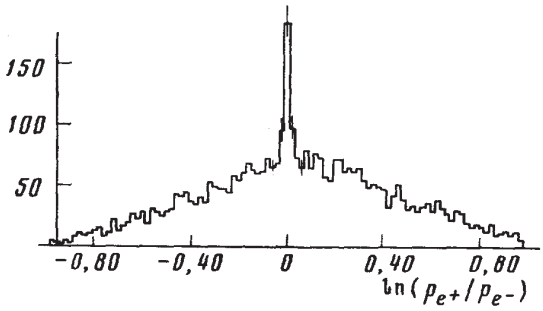

Fig. 10. Distribution of e^+ e^- pairs over $\ln P_{e+}/P_{e-}$. The narrow peak at $\varepsilon = 0$ is the A_{2e} signal

The photon flux and the energy distribution were determined using the (e^+e^-)-pairs produced in this converter. Using the procedure of data process described above 277 ± 40 A_{2e} were identified.

Some of the produced positronia were broken up by interaction in the target matter. Taking into account the positronium formation time one finds that $\varepsilon_1 = (99.2 \pm 0.4)\%$ of the atoms leave the target (note, that if the formation time is neglected, this value would decrease by 17%). When atoms pass the cleaning magnetic field, oscillations occur between the singlet and triplet state [45]. Some of the positronia annihilate because the singlet state decay length is comparable with the channel length. Due to this only $\varepsilon_2 = (89.3 \pm 0.8)\%$ of the atoms reach the spectrometric magnet. Only A_{2e} in the ground state pass the cleaning magnetic field. The number of A_{2e} in the ground state is 83% from the full number of positronia. The final values of ρ_A and ρ_π obtained in [6] are

$$\rho_A = (0.92 \pm 0.14) \cdot 10^{-9} \text{ and } \rho_\pi = (1.84 \pm 0.29) \cdot 10^{-9} \,. \tag{23}$$

These values are in good agreement with theoretical calculation.

3.5 Measurement of the total cross section for interaction of ultrarelativistic positronium atoms with carbon.

The study of the passage of relativistic atoms through matter, permits the investigation of the mechanism of interaction of compound systems at high energies. At present, the theory [50,51] gives a simple energy dependence of the interaction cross sections :

$$\sigma_i(T) = \sigma_{0i}/\beta^2 = \sigma_{0i}\gamma^2(\gamma^2 - 1)^{-1} \,, \tag{24}$$

where β is the velocity of the incident atom in the lab frame, T is its kinetic energy, $\sigma_i(T)$ is the total cross section or the cross section of any possible channel of interaction and σ_{0i} is the asymptotic value of the corresponding cross section. The experimental data on atom-atom collisions has been limited to the value of $\gamma \approx 1.2$. With this γ the cross section for hydrogen interaction with matter is

still about three times greater than the asymptotic value. In the experiment [7] the asymptotic value of the total cross section for positronium interactions with carbon atoms was measured. The setup used in this experiment is described in section 3.4. To obtain data related to the interaction of relativistic positronium with matter in the initial part of the channel, at 2.2 meters from the target, and before the cleaning magnet, a device for installing a $0.1\,\mu$m ($21 \pm 1\,\mu$g/cm^2) thickness carbon film was placed in the beam. After interaction with carbon atoms, A_{2e} could be ionized or excited. In the first case e^+ and e^- were removed from the channel by the cleaning magnet. In the second case, all excited A_{2e} with $\gamma > 230$ were dissociated at the beginning of the cleaning magnet (14) and e^+ and e^- were also removed from the channel. Only A_{2e} in the ground state were detected by the setup. The measurement of the number of A_{2e} in the ground state without absorber and with absorber allows us to obtain the total cross section.

In the experiment, the transmission coefficient, K, for the A_{2e} beam was measured

$$K = (N_A^{\rm abs}/N_A)R\,, \tag{25}$$

where $N_A^{\rm abs}$, N_A are the numbers of detected A_{2e} with and without absorber, and $R = 1.37 \pm 0.07$ is the coefficient taking into account the difference in the time of the measurement with and without absorber. The value of K is

$$K = 0.24 \pm 0.14\,. \tag{26}$$

From (26) and using the description of the superpenetration effect from [10] the asymptotic value of the total cross section for A_{2e} interactions with carbon atoms was obtained

$$\sigma_{tot} = (16^{+\infty}_{-10}) \cdot 10^{-19}\,{\rm cm}^2/{\rm atom}\,. \tag{27}$$

The experimental value is consistent with the theoretical calculation [47] of the asymptotic value $\sigma_{tot}^{th} = 5.7 \cdot 10^{-19}{\rm cm}^2/{\rm atom}$. At the same time the result does not exclude the existence of other mechanisms of ionization or excitation of ultrarelativistic atoms in the medium which would lead to a substantial increase of the cross section (Fig. 11)

4 $\pi^+\pi^-$ atom

The $A_{2\pi}$ lifetime measurement allows one to obtain the difference $|a_0 - a_2|$ of the S-wave $\pi\pi$ scattering lengths with isotope spin 0 and 2 in a model independent way.

4.1 $A_{2\pi}$ production and lifetime

Production of $\pi^+\pi^-$ atoms (and of other hadronic atoms) in inclusive processes was considered and a method of their observation and lifetime measurement was proposed [30]. The atoms are produced in S-states with the cross section:

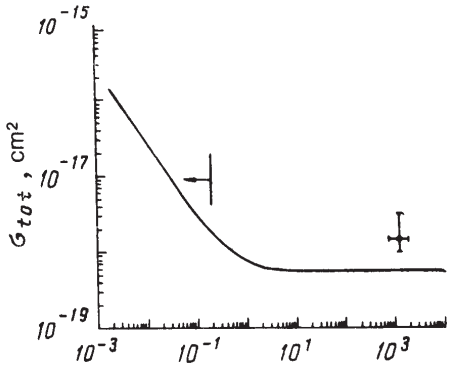

Fig. 11. Total cross section for the interaction of relativistic positronium atoms with carbon as a function of the kinetic energy expressed in the rest masses of the incident atom ($T = \gamma - 1$). The solid curve is the theoretical dependence, • – the measured value. The arrow marks the region ($\gamma < 1.2$) investigated in experiments on the interaction of hydrogen atoms with carbon

$$\frac{d\sigma_n^A}{d\boldsymbol{p}_A} = (2\pi)^3 \frac{E_A}{M_A} |\Psi_n(0)|^2 \frac{d\sigma_0}{d\boldsymbol{p}_1 d\boldsymbol{p}_2} , \tag{28}$$

where $\boldsymbol{p}_A$, E_A and M_A are the momentum, energy and mass of the $\pi^+\pi^-$-atom ($A_{2\pi}$) in the lab system, respectively, $|\Psi_n(0)|^2 = \frac{P_B^3}{\pi n^3}$ is the wave function of $\pi^+\pi^-$ bound state with the Coulomb potential only squared at the origin with the principal quantum number n and the orbital momentum $l = 0$, P_B is the Bohr momentum in $A_{2\pi}$, $d\sigma_0/d\boldsymbol{p}_1 d\boldsymbol{p}_2$ is the double inclusive production cross section for $\pi^+\pi^-$-pairs from short lived sources without taking into account $\pi^+\pi^-$ Coulomb interaction in the final state, $\boldsymbol{p}_1$ and $\boldsymbol{p}_2$ are the π^+ and π^- momenta in the lab system. The momenta of π^+ and π^- mesons obey the relation: $\boldsymbol{p}_1 = \boldsymbol{p}_2 = \frac{\boldsymbol{p}_A}{2}$. The $A_{2\pi}$ are produced in states with different principal quantum numbers n and are distributed according to n^{-3}: $W_1 = 83\%$, $W_2 = 10.4\%$, $W_3 = 3.1\%$, $W_{n\geq 4} = 3.5\%$. The probability of $A_{2\pi}$ production in $K^{\pm}$, K_L^0, η, η', ψ and Υ mesons decay were calculated in [34].

The lifetime τ_n of $A_{2\pi}$ with the principal quantum number n and $l = 0$, is determined by the charge-exchange process $\pi^+\pi^- \to \pi^0\pi^0$ and, at the leading order of isospin breaking, may be described through the S-wave $\pi\pi$ scattering lengths a_0 and a_2 with isospin values 0 and 2 [13,14]:

$$\frac{1}{\tau_n} = \frac{8\pi}{9} \left(\frac{2\Delta m}{\mu}\right)^{\frac{1}{2}} (a_0 - a_2)^2 |\Psi_n(0)|^2 , \tag{29}$$

where $\Delta m = M_A - 2m_{\pi^\circ}$, m_{π° is π^0-meson mass and μ is $A_{2\pi}$ reduced mass. The lifetime dependence on n is determined by $|\Psi_n(0)|^2$ value and from (29) one obtains $\tau_n = \tau_1 \cdot n^3$. It follows from (29) that the τ_1 measurement with 10%

precision would allow one to determine $|a_0 - a_2|$ in a model independent way, with 5% precision. The corrections to (29) were obtained in [52,16,15,17,53]. In the work [53], the electro-magnetic interactions and the mass difference of the u and d quarks as isospin breaking effects was evaluated to improve the expression for the lifetime of $A_{2\pi}$:

$$\frac{1}{\tau_n} = \frac{8\pi}{9}\left(\frac{2\Delta m}{\mu}\right)^{\frac{1}{2}} (a_0 - a_2 + \varepsilon)^2 \, |\Psi_n(0)|^2(1+K) \,, \tag{30}$$

where values of ε and K are around 10^{-2}. Corrections to relation (29) have also been studied in a potential approach [54,55].

In the chiral perturbation theory [18] one finds [56,57,23]: $a_0 - a_2 = (0.265 \pm 0.004) m_\pi^{-1}$. Inserting $a_0 - a_2$ to (30) one can calculate $\tau_1 = (2.90 \pm 0.09) \cdot 10^{-15}$ s.

4.2 $A_{2\pi}$ detection method and setup description

The experiment on the observation of $\pi^+\pi^-$ atoms was carried out at the 70 GeV proton synchrotron (U-70) at Serpukhov [31,32]. Pionic atoms and $\pi^+\pi^-$ pairs ("free" pairs) were produced in a 8 μm thick tantalum target ("thick" target) inserted into the internal proton beam. The atoms can either annihilate into $\pi^0\pi^0$ pairs or break up (ionize) into $\pi^+\pi^-$ pairs ("atomic" pairs) inside the same target. The "free" and "atomic" pairs get into the 40 m long vacuum channel (the acceptance is $3.8 \cdot 10^{-5}$ sr) at 8.4° to the proton beam and are detected by the setup in the $0.8 \div 2.4$ GeV/c pion momentum interval.

The number of "atomic" pairs depends on the atom lifetime τ, the cross section of atom-atom interactions [46,47,58,59,60,61,62,63,64,65,66,67,68,69] and the target thickness. By calculating the probability of the $A_{2\pi}$ breakup [70] and measuring the number of "atomic" pairs it is possible to obtain the $A_{2\pi}$ lifetime [30,32]. Assuming $\tau_1 = 3.0 \cdot 10^{-15}$ s the annihilation length of $A_{2\pi}$ in the $1S$-state at $\gamma = 10$ is 9 μm and the $A_{2\pi}$ mean free path in Ta is 6 μm independent of the γ factor for $\gamma > 6$. In this experiment, on average 8 atoms were generated per 10^{11} p-Ta interactions into the setup acceptance and ∼40% of the atoms broke up in the target into "atomic" pairs detected by the setup. The checking measurements were carried out with a 1.4 μm thick tantalum target ("thin" target), where only ∼ 10% of the atoms broke up. Pions in "atomic" pairs have a small relative momenta $Q < 3$ MeV/c in c.m.s., and therefore approximately equal energies $E_+ \approx E_-$ in the lab system and a small opening angle $\Theta_{1,2} \approx 6/\gamma$ mrad.

The experimental setup shown in Fig. 12 has a relative momentum resolution of about 1 MeV/c. The channel is connected to the accelerator vacuum pipe without any partition and is shielded against the accelerator and the Earth magnetic fields. The channel ends with a vacuum chamber placed between the spectrometer magnet poles ($B = 0.85$ T).

Charged particles were detected by the telescopes T_1 and T_2. The track coordinates were measured by drift chambers. The time interval between detector hits in T_1 and T_2 was measured by scintillation hodoscopes. Electrons and positrons were rejected by gas Cherenkov counters, and muons by scintillation

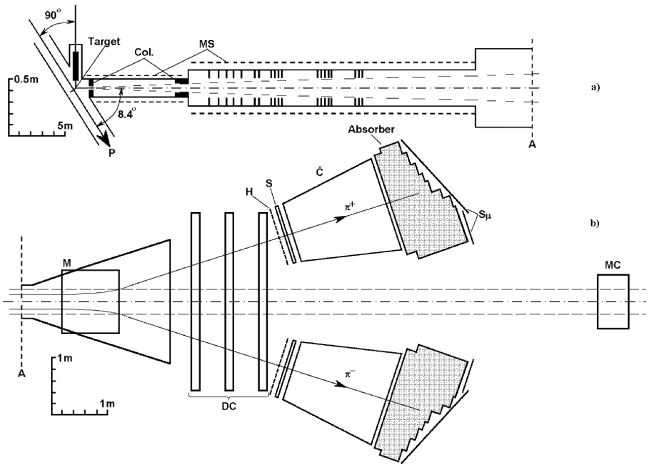

Fig. 12. Experimental setup for observation $A_{2\pi}$: (a) – channel scheme: p – internal proton beam, $Target$ – target mechanism, Col – collimator, MS – magnetic shield; (b) – magnet and detectors: M – poles of spectrometer magnet, VC – vacuum chamber, DC – drift chambers, H – scintillation hodoscopes, S,S_μ – scintillation counters, C – gas Cherenkov counters, $Absorber$ – cast-iron absorber, MC – monitor counters

counters placed behind absorbers. Besides π mesons other charged hadrons were also detected.

The measurements and simulation allowed us to obtain the setup resolution of the momentum $\sigma_p/p = 0.008$, on the vertical plane angle of deviation from the target direction $\sigma_{\varphi_1} = \sigma_{\varphi_2} = 1.2\,\text{mrad}$ and on the angle between particles at the magnet entrance $\sigma_{\theta_{1,2}} = 0.1\,\text{mrad}$. Also were obtained the distributions of "atomic" pairs on the Q projections to $\boldsymbol{p} = \boldsymbol{p}_1 + \boldsymbol{p}_2$ direction (Q_L) and to the plane perpendicular to $\boldsymbol{p}$ (Q_T). The distributions of Q_L and of Q_T components Q_X and Q_Y are Gaussian-like and have the standard deviations $\sigma_{Q_L} = 1.3\,\text{MeV}/c$, $\sigma_{Q_X} = \sigma_{Q_Y} = 0.60\,\text{MeV}/c$ for the "thick" target and $\sigma_{Q_L} = 1.3\,\text{MeV}/c$, $\sigma_{Q_X} = \sigma_{Q_Y} = 0.44\,\text{MeV}/c$ for the "thin" target. The momentum resolution and all standard deviations are averaged in $0.8 \div 2.4\,\text{GeV}/c$ pion momentum range.

4.3 Data processing

At data processing a space reconstruction of events was fulfilled. The particle momenta and the track coordinates at the magnet entrance were calculated under the assumption that the particles came from the target. Pairs originating in the target were selected by applying the requirement that vertical projections of tracks must "look" on the target.

The selected events are distributed in the time difference t_H between hits of the hodoscopes as shown in Fig. 13. The distribution contains the true coincidence peak ($\sigma = 0.8\,\text{ns}$) and the uniform background from accidental coinci-

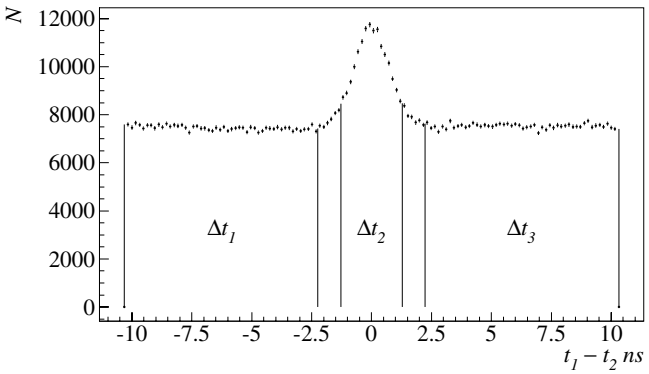

Fig. 13. Distribution of the time difference between hits in the hodoscopes. The peak is formed by time-correlated $\pi^+\pi^-$-pairs, and the uniform background is due to accidental coincidences

dences. The intervals $\Delta t_1 = \Delta t_3 = 8.0\,\text{ns}$ were used to determine the number of accidental events N_a in the signal region, and the interval $\Delta t_2 = 2.56\,\text{ns}$ to obtain the sum N_{ta} of true and accidental events. In the interval Δt_2 the ratio of true to accidental events is 0.36. The true coincidences N_t are caused mainly (97%) by $\pi^+\pi^-$ pairs produced in the target.

In order to get a better separation of the "atomic" from the "free" pairs we analyzed the distribution of the events in the variable F instead of Q:

$$F = \sqrt{\left(\frac{Q_L}{\sigma_{Q_L}}\right)^2 + \left(\frac{Q_X}{\sigma_{Q_X}}\right)^2 + \left(\frac{Q_Y}{\sigma_{Q_Y}}\right)^2}\,. \tag{31}$$

The true event distribution in F (and in other variables) was found from the obvious relation:

$$\frac{dN_t}{dF} = \frac{dN_{ta}}{dF} - \left[\frac{\Delta t_2}{\Delta t_1 + \Delta t_3}\right] \cdot \frac{dN_a}{dF}\,. \tag{32}$$

The distribution (32) was fitted for $F > 3$ (where "atomic" pairs are absent) by an approximating distribution. The number of "atomic" pairs is then determined by the difference between the number of $\pi^+\pi^-$ pairs in the interval $F < 2$ and the corresponding number of "free" pairs, obtained for $F < 2$ by an extrapolation of the curve fitted to the data in the region $F > 3$.

4.4 Approximation procedure for the $\pi^+\pi^-$ pair distribution $A_{2\pi}$ number obtaining

To obtain the approximation of the "free" pair distribution we have taken as a base the accidental $\pi^+\pi^-$ pair distribution $dN_a^{\pi\pi}/dF \equiv \Phi(F)$ because the latter and the true $\pi^+\pi^-$ pair distribution dN_t^0/dF, without taking into account the

final state interaction, should have the same shape. Therefore, dN_t^0/dF equals to $\Phi(F)$.The distribution $\Phi(F)$ was obtained from the accidental event distribution dN_a/dF by subtracting the $\pi^- p$ and πK accidental pairs.

The distribution $\Phi(F)$ is a sum of the "Coulomb" pair distribution from short lived sources (pairs from direct processes and from decays of $\rho, \omega, \varphi, ...$) and of the "non-Coulomb"pair distribution from long lived sources (one or both π mesons arise from η or K_S^0 decays).

The typical size of the pion production region in the case of short lived sources is $1 \div 3$ fm which is much smaller than the Bohr radius of the $\pi^+\pi^-$ atom ($r_B = 387$ fm). Thus the Coulomb interaction in the final state was taken into account multiplying $\Phi(F)$ with the Coulomb factor $A_C(\beta)$ [71] which depends on the relative velocity β of the $\pi^+\pi^-$ pair in its c.m.s.:

$$A_C(\beta) = \frac{2\pi\eta}{\exp(2\pi\eta) - 1}, \quad \eta = -\alpha/\beta, \;\; \alpha = 1/137 \, . \tag{33}$$

The corrections caused by the strong interaction were not introduced into this distribution because the corresponding correlation function in the analyzed interval of F differs from a constant by a few percent [72]. The pion pairs from long lived sources do not interact in the final state, and therefore no correction to the distribution $\Phi(F)$ was applied.

From above we can write the approximating distribution in the form:

$$\frac{dN_t}{dF} = q\Phi(F)[A_C(\beta) + f] \, , \tag{34}$$

where q is a normalization factor; f is a free parameter which accounts for the "non-Coulomb" pair fraction.

In the interval $0 \le F \le 40$ the distributions dN_t/dF for "thick" and "thin" targets are shown as points with errors in Fig. 14(a) and 14(c) and contain $5.9 \cdot 10^4$ and $4.4 \cdot 10^4$ events respectively. To improve the statistical precision, the distributions for "thick" and "thin" targets were fitted jointly by the distribution (34), as the parameter f does not depend on the target thickness. The parameter value was found: $f = 1.8 \pm 0.3$. The fitting distributions (34) for events obtained for "thick" and 'thin" targets are also presented in Fig. 14(a) and 14(c) as histograms. The ratios of the experimental distribution for the "thick" and "thin" targets are shown in Fig. 14(b) and 14(d).

The following numbers of excessive pairs for the "thick", n_A^{tk}, and the "thin" target, n_A^{tn}, in the interval $F \le 2$ were obtained:

$$n_A^{tk} = 272 \pm 49, \quad \overline{\chi^2} = 1.28; \quad n_A^{tn} = 35 \pm 41, \quad \overline{\chi^2} = 0.75 \, . \tag{35}$$

The excessive pair number for the "thin" target, normalized to the proton interaction number for "thick" target, is $n_A^{tn} = 47 \pm 55$.

4.5 Status of $A_{2\pi}$ investigation at CERN

The DIRAC experiment at CERN [73] aims to measure the lifetime of $\pi^+\pi^-$ atoms in the ground state with 10% precision, to obtain the value $|a_0 - a_2|$ with

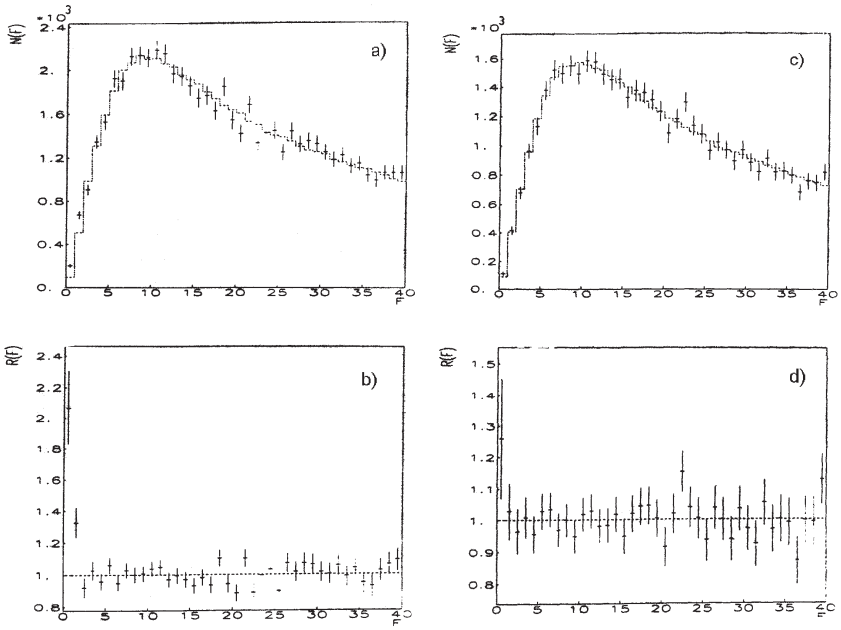

Fig. 14. Experimental distribution of $\pi^+\pi^-$ pairs produced in the "thick" (a) and "thin" (c) targets as a function of F (points with errors) and approximating distributions of "free" pairs on the same variable (dashed histogram); the ratio of the experimental to the approximating distribution for "thick" (b) and "thin" (d) targets. The deviation of the ratio from unity in the two first bins in (b) is due to extra pairs originating from ionization of $A_{2\pi}$ in the "thick" target. The absence of extra pairs in the first two bins in (d) is caused by the low $A_{2\pi}$ ionization probability in the "thin" target

an accuracy of 5%, and to submit the understanding of chiral symmetry breaking of QCD to a crucial test. At present time, the $\pi\pi$ scattering is also studied in the experiments E865 at Brookhaven and KLOE at DAΦNE in K_{l4} decays.

The experimental setup (Fig. 15) is located at the PS CERN extracted proton beam with the energy of 24 GeV. The atomic and free pairs arising in the target (Be, Ti, Ni or Pt) get into the secondary particle channel. The experimental setup is a magnetic spectrometer with coordinate detectors aligned upstream from the spectrometer magnet near the target, and two telescope arms for positively and negatively charged particles downstream of the magnet. The coordinate detectors are the microstrip gas chambers, scintillation fibre detector and scintillation ionization hodoscope. Each telescope is equipped with the drift chambers, horizontal and vertical hodoscopes, gas Cherenkov counter and muon detector. The last two detectors are used to suppress detection of electrons and muons, correspondingly. The relative momentum resolution of the setup is about 1 MeV/c. The required accuracy of the setup on relative momentum is provided

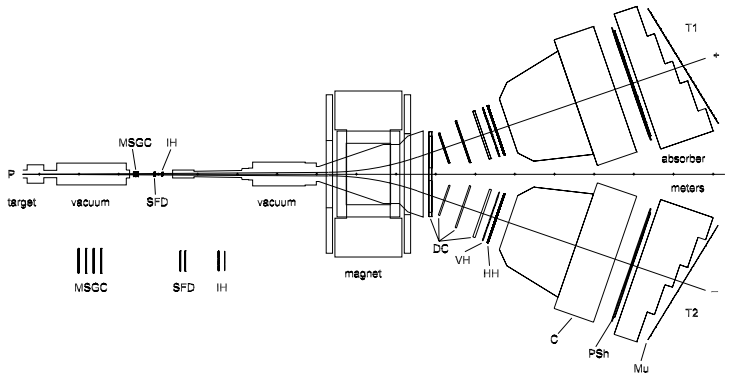

Fig. 15. Schematic top view of the DIRAC spectrometer. Moving from the target station toward the magnet there are: four MicroStrip Gas Chambers (MSGC), two Scintillating Fibre Detectors (SFD) and an Ionization Hodoscope (IH). Located downstream from the dipole magnet, on each arm of the spectrometer, are: 4 modules of Drift Chambers (DC), a Vertical and a Horizontal Hodoscope (VH, HH), a Cherenkov counter (C), a Preshower detector (PSh) and, behind an iron absorber, a Muon counter (Mu)

by high resolution of the coordinate detectors and a small quantity of materials on a particle way. The collection of data for a lifetime measurement with 10% precision is planned for 2001–2002.

4.6 $A_{\pi K}$ as a source of model-independent data on πK S-wave scattering lengths

The dominant decay process for $A_{\pi K}$ is:

$$A_{\pi K} \to \pi^0 + \overline{K^0}\,. \tag{36}$$

For $A_{\pi K}$ with principal quantum number n and orbital angular momentum $l = 0$, the probability for this transition at leading order of isospin breaking is given by the expression [14]:

$$W_{n,0}(\pi^0\overline{K^0}) = \frac{1}{\tau_{n,0}} \approx A\,(a_{1/2} - a_{3/2})^2\,, \tag{37}$$

where $a_{1/2}$ and $a_{3/2}$ are the S-wave πK scattering lengths with the isotop spin $1/2$ and $3/2$ and A is known constant.

Substituting the πK scattering length values from [74] into (37), one obtains, at leading order in isospin breaking, the $A_{\pi K}$ lifetime in the ground state $\tau_{1,0} \equiv \tau = 4.7 \cdot 10^{-15}$ s.

By measuring the annihilation probability of the atom and knowing the distribution of $A_{\pi K}$ as a function of n, using the same method as in the case of

$A_{2\pi}$, we can obtain the lifetime τ and, finally, extract a value for $|a_{1/2} - a_{3/2}|$ [30].

The $A_{\pi K}$ yield from proton-nucleus interaction at $24 \div 450\,\mathrm{GeV}$ was calculated in [33].

Acknowledgements

The author wishes to thank L.Afanasyev and A.Kuptsov for their help with this review, and C.Moine and A.Rodrigues Fernandez for the preparation of the text.

References

1. L.L. Nemenov: Yad.'Fiz. **16**, 125 (1972); Sov. J. Nucl. Phys. **16**, 67 (1972)
2. R. Coombes et al.: Phys. Rev. Lett. **37**, 249 (1976)
3. S.H. Aronson et al.: Phys. Rev. **D33**, 3180 (1986)
4. L.L. Nemenov: Yad. Fiz. **15**, 1047 (1972); Sov. J. Nucl. Phys. **15**, 582 (1972)
5. G.D. Alekseev et al.: Yad. Fiz. **40**, 139 (1984); Sov.J.Nucl.Phys. **40**, 87 (1984)
6. L.G. Afanasyev et al.: Phys. Lett. **B236**, 116 (1990); L.G. Afanasyev et al.: Yad.Fiz. **51**: 1040 (1990); Sov. J. Nucl. Phys. **51**, 664 (1990)
7. L.G. Afanasyev et al.: Yad. Fiz, **50**, 7 (1989); Sov. J. Nucl. Phys. **50**, 4 (1989)
8. L.L. Nemenov: Yad. Fiz. **34**, 1306 (1981); Sov. J. Nucl. Phys. **34**, 726 (1981)
9. V.L. Lyuboshits and M.I. Podgoretskiĭ: Zh. Eksp.Teor. Fiz. **81**, 1556 (1981); Sov. Phys. JETP **54**, 827 (1981)
10. A.S. Pak, A.V. Tarasov: Sov. J. Nucl. Phys. **45**, 92 (1987); Yad. Fiz. **45**, 145 (1987)
11. B.G. Zakharov: Yad. Fiz. **46**, 148 (1987);
12. L.L. Nemenov: Yad. Fiz. **51**, 444, (1990); Sov. J. Nucl. Phys. **51**, 284 (1990)
13. J. Uretsky and J. Palfrey: Phys.R ev. **121**, 1798 (1961)
14. S.M. Bilenky et al.: Yad. Fiz. **10**, 812 (1969); Sov. J. Nucl. Phys. **10**, 469 (1970)
15. H. Jallouli and H. Sazdjian, Phys. Rev. **D58**, 014011 (1998); Erratum: *ibid.*, **D58**, 099901 (1998)
16. M.A. Ivanov, V.E. Lyubovitskij, E.Z. Lipartia and A.G. Rusetsky: Phys. Rev. **D58**, 0094024 (1998).
17. A. Gall, J. Gasser, V.E. Lyubovitskij and A. Rusetsky: Phys. Lett. **B462**, 335 (1999)
18. For reviews on CHPT see e.g. H.L eutwyler [21]; U.G. Meißner: Rep.Prog. Phys. **56** (1993) 903; A. Pich: Lectures given at the V Mexican School of Particles and Fields, Guanajuato, México, December 1992, preprint CERN-Th.6978/93 (hep-ph/9308351); G. Ecker: 'Chiral perturbation theory'. In: *Quantitative Particle Physics* Cargèse 1992, Eds. M. Lévy et al. (Plenum Publ. Co., New York, 1993) pp. 101-148; J.F. Donoghue, E. Golowich and B.R. Holstein: *Dynamics of the Standard Model* (Cambridge University Press, Cambridge 1992)
19. S. Weinberg, Physica **96A**, 327 (1979)
20. J. Gasser and H. Leutwyler: Phys. Lett. **125B**, 327 (1983)
21. H. Leutwyler: 'Nonperturbative Methods'. In: Proc. XXVI Int. Conf. on High Energy Physics, Dallas, 1992, ed. by J.R. Sanford, AIP Conf. Proc. No. 272 (AIP, New York, 1993) pp. 185–211
22. H. Leutwyler, Ann. Phys. **235**, 165 (1994); hep-ph/9311274

23. G. Colangelo, J. Gasser and H. Leutwyler: Phys. Lett. **B488**, 261 (2000)
24. M. Gell-Mann, R.J. Oakes and B. Renner: Phys. Rev. **175**, 2195 (1968)
25. S. Glashow and S. Weinberg, Phys. Rev. Lett. **20**, 224 (1968)
26. M.H. Fuchs, H. Sazdjian and J. Stern: Phys. Lett. **B269**, 183 (1991)
27. J. Stern, H. Sazdjian and N.H. Fuchs: Phys. Rev. **D47**, 3814 (1993); M. Knecht and J. Stern: 'Generalized Chiral Perturbation Theory'. In: *DAPHNE Physics Handbook* 2nd edn., ed. by L. Maiani, G. Pancheri and N.Paver, pp 169–190; hep-ph/9411253
28. M. Knecht et al.: Nucl. Phys. **B457**, 513 (1995)
29. H. Sazdjian: Phys. Lett. **B490**, 203 (2000); hep-ph/0004226
30. L.L. Nemenov: Yad. Fiz. **41**, 980 (1985); Sov. J. Nucl. Phys. **41**, 629 (1985)
31. L.G. Afanasyev et al.: Phys. Lett. **B308** 200 (1993)
32. L.G. Afanasyev et al.: Phys. Lett. **B338**: 478 (1994)
33. O.E. Gorchakov, A.V. Kuptsov, L.L. Nemenov and D.Yu. Riabkov: Yad. Fiz. **63**, 1936 (2000); Phys.Atom.Nucl. **63**, 1847 (2000)
34. Z.K. Silagadze: JETP Lett. **60**, 689 (1994); hep-ph/9411382
35. R. Staffin: Phys. Rev. **D 16**, 726 (1977)
36. Ching Cheng-rui, Ho Tso-hsiu, and Chang Chao-hsi: Phys. Lett. **B98**, 456 (1981)
37. U. Barr-Gadda and C.F. Cho: Phys. Lett. **B46**, 95 (1973); C.F. Cho: Nuovo Cimento **A23**, 557 (1974); H.M.M. Mansour and K. Higgins: *ibid.*, **A36**, 95 (1976); A. Karimkhodzhaev and R.N. Faustov: Yad. Fiz. **29**, 463 (1979); Sov. J. Nucl. Phys. **29**, 232 (1979)
38. C.F. Cho: Nuovo Cimento **A23**, 557 (1974)
39. H.M.M. Mansour and K. Higgins: Nuovo Cimento **A36**, 196 (1976).
40. A. Karimkhodzhaev and R.N.Faustov, Yad. Fiz. **29**, 463 (1979); Sov. J. Nucl. Phys. **29**, 232 (1979)
41. S.H. Aronson et al.: Phys.Rev.Lett. **48**, 1078 (1982)
42. M.I. Vysotskii: Yad. Fiz. **29**, 845 (1979); Sov. J. Nucl. Phys. **29**, 434 (1979)
43. O.E. Gorchakov, A.V. Kuptsov, and L.L. Nemenov: Yad. Fiz. **24**, 524 (1976); Sov. J. Nucl. Phys. **24**, 273 (1976)
44. G.V.M eledin, V.G. Serbo and A.K. Slivkov: Pis'ma Zh. Exp. Teor. Fiz **13**, 98 (1971); JETP Lett. **13**, 68 (1971)
45. L.L. Nemenov: Yad. Fiz. **24**, 319 (1976); Sov. J. Nucl. Phys. **24**, 166 (1976)
46. L.S. Dul'yan and A.M. Kotsinyan: Yad. Fiz. **37**, 137 (1983); Sov. J. Nucl.P hys. **37**, 78 (1983)
47. A.S. Pak, A.V. Tarasov: JINR-P2-85-903, Dubna 1985.
48. H.A. Olsen: Phys. Rev. **D 33**, 2033 (1986)
49. V.L. Lyuboshits: Yad. Fiz. **45**, 1099 (1987); Sov. J. Nucl. Phys. **45**, 682 (1987)
50. G.H. Gillespie: Phys. Rev. **A18**, 1967 (1978)
51. G.H. Gillespie and M.Inokuti: Phys. Rev. **A22**, 2430 (1980)
52. V.E. Lyubovitskij, E.Z. Lipartia and A.G. Rusetsky: Pis'ma Zh. Exp. Teor. Fiz **66**, 747 (1997); JETP Lett. **66** 783
53. J. Gasser, V.E. Lyubovitskij and A.G. Rusetsky: Phys. Lett. **B471**, 244 (1999)
54. U. Moor, G. Rasche and W.S. Woolcock, Nucl. Phys. **A587**, 747 (1995)
55. A. Gashi et al.: Nucl. Phys. **A628**, 101 (1998)
56. J. Bijnens et al.: Phys. Lett. **B374**, 210 (1996)
57. J. Bijnens et al.: Nucl. Phys. **B508**, 263 (1997)
58. S. Mrowczynski: Phys. Rev. **A33**, 1549 (1986)
59. S. Mrowczynski: Phys. Rev. **D36**, 1520 (1987)
60. K.G. Denisenko and S. Mrowczynsky: Phys. Rev. **D36**, 1529 (1987)

61. A.V. Kuptsov, A.S. Pak and S.B. Saakian: Yad. Fiz. **50**, 936 (1989); Sov. J. Nucl. Phys. **50**, 583 (1989)
62. L.G. Afanasyev: JINR-E2-91-578, Dubna 1991
63. L.G. Afanasyev and A.V. Tarasov: JINR E4-93-293, Dubna, 1993
64. L.G. Afanasyev: Atomic Data and Nuclear Data Tables, **61**, 31 (1995)
65. Z. Halabuka et al.: Nucl. Phys. **554**, 86 (1999)
66. A.V. Tarasov and I.U. Christova, JINR P2-91-10, Dubna, 1991
67. O.O. Voskresenskaya, S.R. Gevorkyan and A.V. Tarasov: Yad. Fiz. **61**, 1628 (1998); Phys.Atom.Nucl. **61**, 1517 (1998)
68. L. Afanasyev, A. Tarasov and O. Voskresenskaya: J. Phys. **G 25**, B7 (1999)
69. D.Yu. Ivanov and L. Szymanowski: Eur. Phys. J.**A5**, 117 (1999)
70. L.G. Afanasyev and A.V. Tarasov: Yad. Fiz. **59**, 2212 (1996); Phys. Atom. Nucl. **59**, 2130 (1996)
71. A.D. Sakharov: Zh. Eksp.Teor.Fiz. **18**, 631 (1948)
72. L.G. Afanasyev et al.: Yad. Fiz. **52**: 1046 (1990); Sov. J. Nucl. Phys. **52** 666 (1990); L.G.Afanasyev et al.: Phys.Lett. **B255**, 146 (1991)
73. B. Adeva et al.: CERN/SPSLC 95–1, SPSLC/P 284, Geneva 1995.
74. V. Bernard, N. Kaiser and U. Meissner: Phys. Rev. **D43**, 2757 (1991); V. Bernard, N. Kaiser and U. Meissner, Nucl. Phys. **B357**, 129 (1991)